Homodyne *en face* optical coherence tomography

Zahid Yaqoob

Department of Electrical Engineering, MC 136-93, California Institute of Technology, Pasadena, California 91125

Jeff Fingler

Department of Applied Physics, MC 139-74, California Institute of Technology, Pasadena, California 91125

Xin Heng and Changhuei Yang

Department of Electrical Engineering, MC 136-93, California Institute of Technology, Pasadena, California 91125

We demonstrate, for what we believe to be the first time, the use of a 3×3 fiber-optic coupler to realize a homodyne optical coherence tomography (OCT) system for *en face* imaging of highly scattering tissues and turbid media. The homodyne OCT setup exploits the inherent phase shifts between different output ports of a 3×3 fiber-optic coupler to extract amplitude information of a sample. Our homodyne *en face* OCT system features a measured resolution of 14 μm axially and 9.4 μm laterally with a 90 dB signal-to-noise ratio at 10 μs integration time. *En face* OCT imaging of a stage 52 *Xenopus laevis* was successfully demonstrated at a depth of 600 μm within the sample. © 2006 Optical Society of America

OCIS codes: 170.0180, 170.4500, 170.3880.

Optical coherence tomography (OCT) is a noninvasive technique for high-resolution depth-resolved imaging of highly scattering biological samples.[1] *En face* OCT systems[2,3] belong to a special class of OCT that preferentially provides sample images in a plane normal to the optical axis. The reported *en face* OCT systems can be categorized into two types: full-field OCT designs[3] and two-dimensional (2D) beam scanning designs.[2,4] Most of the reported *en face* OCT systems use heterodyne techniques to measure the interference signal.[2–4] The use of a heterodyne carrier frequency requires a minimum dwell time (equal to one full oscillation period) for each pixel acquisition. We note that a homodyne-detection-based *en face* OCT system can be simpler to implement and does not impose a dwell time requirement. Beaurepaire *et al.*[5] reported such a system. However, in that system the amplitude and phase information are entangled. In this Letter we present a 3×3 fiber-optic-coupler-based homodyne OCT system that is capable of obtaining the amplitude independent of the phase information. This *en face* OCT system exploits the nontrivial phase shift in a 3×3 fiber-optic coupler, which permits simultaneous and independent acquisition of the sample phase and amplitude information.[6] The proposed design is simple, easy to implement, and offers a low-cost and high-speed *en face* imaging solution.

Figure 1(a) shows the design of our 3×3 fiber-optic coupler-based homodyne *en face* OCT system. A broadband light source (SuperlumDiodes Ltd., D1300-HP) of $\lambda_0 = 1300$ nm, $\Delta\lambda \sim 85$ nm is coupled to a 3×3 coupler (AC Photonics) via a 2×2 coupler (AC Photonics). A 2D mirror scanner (Physik Instrumente, S-334.2SL) in the sample arm is used to scan the sample beam. A $4f$ lens system ($f = 150$ mm) along with a $20 \times$ microscope objective (Olympus, LMPLAN IR) helps to achieve linear scanning across the

sample. Light returning from the sample and reference arms is collected by three detectors (New Focus Model 2011) marked D_1, D_2, and D_3. A similar detector (D_4) is used to measure source intensity; the measurement can then be used to correct for the source fluctuations. The data are acquired by using a 16-bit analog-to-digital converter (National Instruments, PXI-6120).

To facilitate our explanation of the homodyne OCT concept, we first define a set of coefficients α_{mn}, where α_{mn} denotes the power transfer coefficient from port m to port n of the 3×3 coupler. By the na-
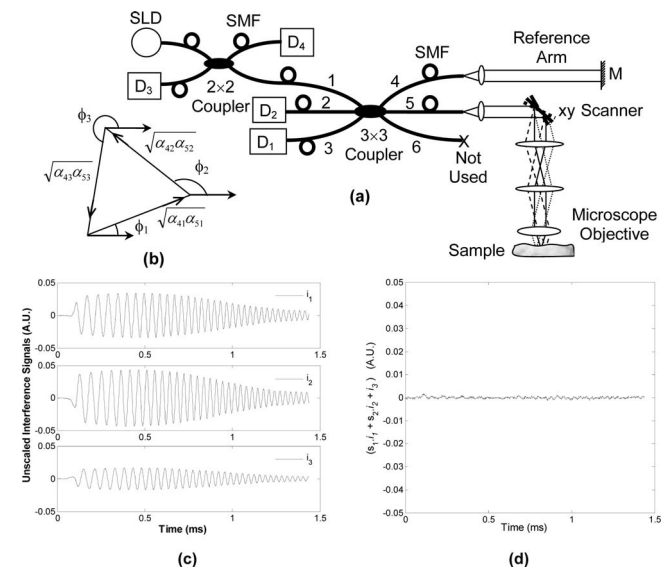

Fig. 1. (a) Schematic of homodyne *en face* OCT system. (b) Schematically demonstrates triangular relationship between 3×3 coupler coefficients and interferometric phase shifts between the coupler arms. (c) Unscaled interference signals at detectors D_j after dc removal. (d) Sum of the scaled interference signals. SLD, superluminescent diode; SMF, single-mode fiber; i_j, jth interference signal.

ture of the fiber coupler, reciprocity ($\alpha_{mn} = \alpha_{nm}$) applies. The optical signal detected by the jth detector can be expressed as

$$P_j(z) = P_{r,j} + P_{s,j} + 2(1/s_j)\sqrt{\alpha_{41}\alpha_{4j}\alpha_{51}\alpha_{5j}}\sqrt{P_r}$$
$$\times\{\sqrt{P_s(z)} \otimes \gamma(z)\}\cos[2k_0 z + \psi(z) + \phi_j], \quad (1)$$

where $P_{r,j}$ and $P_{s,j}$ represent the total measured power from the reference and sample arms, respectively; $1/s_j$ is the loss scale factor that accounts for coupler loss and detector loss to the detected interferometric signal. The factors P_r, $P_s(z)$, and $\gamma(z)$ are the returning reference power, the returning coherent light from depth z in the sample, and the autocorrelation function of the broadband light source, respectively. k_0 is the optical wavenumber (corresponding to the center wavelength) in air, and $\psi(z)$ is the intrinsic reflection phase shift of the sample at depth z. The interferometric phase shift ϕ_j differences are dependent on the relative values of α_{mn}; for example, if α_{mn} are all equal (ideal equal-split coupler), the two ϕ_j should differ from each other by 120°. The method of extracting complex interferometric signal components from such homodyne measurements works as long as none of the differences between ϕ_j are equal to 0° or 180°.[6]

We define i_j as the interferometric portion of $P_j(z)$. Assigning $s_1 i_1$ as the real part of the complex interferometric signal (set $\phi_1 = 0$), the real and imaginary parts of the interference signal can then be written as[6]

$$i_{\text{Re}} = s_1 i_1 = 2\sqrt{\alpha_{41}\alpha_{41}\alpha_{51}\alpha_{51}}\sqrt{P_r}\{\sqrt{P_s(z)} \otimes \gamma(z)\}$$
$$\times\cos[2k_0 z + \psi(z)], \quad (2a)$$

$$i_{\text{Im}} = 2\sqrt{\alpha_{41}\alpha_{41}\alpha_{51}\alpha_{51}}\sqrt{P_r}\{\sqrt{P_s(z)} \otimes \gamma(z)\}$$
$$\times\sin[2k_0 z + \psi(z)],$$
$$= \frac{s_1 i_1 \cos(\phi_2) - s_2 i_2 \beta}{\sin(\phi_2)}, \quad \text{where } \beta = \sqrt{\frac{\alpha_{41}\alpha_{51}}{\alpha_{42}\alpha_{52}}}. \quad (2b)$$

The derivation of Eq. (2b) is detailed in Ref. 6. Complete quadrature information (amplitude and phase) can be simultaneously obtained as

$$i_0 = \sqrt{i_{\text{Re}}^2 + i_{\text{Im}}^2}, \quad (3a)$$

$$2k_0 z + \psi(z) = \tan^{-1}(i_{\text{Im}}/i_{\text{Re}}). \quad (3b)$$

To use Eqs. (2) and (3), we have to experimentally quantify the coefficients β, ϕ_j, and s_j. As we are primarily interested in the relative magnitudes of s_j, we can make a simplifying assumption that $s_3 = 1$. We quantify all of these parameters through a calibration process in which we replace the sample with a mirror. A slight tilt in the sample mirror results in phase modulation in our detected signals as the sample beam scans across the mirror. At each detector, two sets of 3000 sample points were acquired at 80 kHz with the reference arm blocked (to determine

$P_{s,j}$) and unblocked. A knife-edge introduced into the sample arm blocks the sample light for a fraction of each scan, allowing $P_{r,j}$ to be measured. The two data sets were offset balanced and subtracted to determine the interference signals at the three detectors [see Fig. 1(c)]. The three interferometric signals should add up to zero by the law of power conservation.[6] This condition enables us to determine the scaling factors s_1 and s_2 in our experimental situation. Specifically, we can write a matrix

$$\begin{bmatrix} i_1(t_1) & i_2(t_1) \\ i_1(t_2) & i_2(t_2) \end{bmatrix}\begin{bmatrix} s_1 \\ s_2 \end{bmatrix} = -\begin{bmatrix} i_3(t_1) \\ i_3(t_2) \end{bmatrix}, \quad (4)$$

where $i_j(t_1)$ and $i_j(t_2)$ are the three interferometric signal values at two different time instances. We find the best fit values for factors s_1 and s_2 by inserting multiple sets of interferometric data points into Eq. (4). Figure 1(d) shows a representative plot of the sum of the scaled interference signals. Knowing the value of each s_j, the values of the peak fringe height from each scaled interferometric signal, $s_j i_j$, which are proportional to $\sqrt{\alpha_{4j}\alpha_{5j}}$ [see Fig. 1(b)], can then be used to determine β as well as ($\phi_j - \phi_k$). Four sets of coupler characterizations were performed at different times, which yielded an averaged β of 0.95 ± 0.01 and the interferometric phase shifts ($\phi_j - \phi_k$) at $122.7° \pm 0.2°$, $121.1° \pm 0.8°$, and $116.2° \pm 0.7°$, respectively.

To construct the homodyne OCT signal, the reference arm dc power $P_{r,j}$ is first subtracted from the measured detector power $P_j(z)$. Next, the summation $\Sigma_{k=1}^3 s_k[P_k(z) - P_{r,k}]$, with s_3 set as 1, removes all the interference terms, leaving only the sum of the scaled contributions from the sample dc power of all the detectors. Assuming that the instantaneous ratio of the measured sample power of the detectors is equal to the average ratio of the measured sample power of each detector, the instantaneous scaled sample power measured in each detector is determined by

$$s_j P_{s,j} = \frac{\sum_k s_k[P_k(z) - P_{r,k}]}{\sum_k (\langle P_{s,k}\rangle/\langle P_{s,2}\rangle)} \frac{\langle P_{s,j}\rangle}{\langle P_{s,2}\rangle}. \quad (5)$$

Removing the values of Eq. (5) from the scaled reference-removed measurements, the remaining terms are the scaled interference signals $s_j i_j$. The OCT signal can then be determined by using Eq. (3a).

Our proof-of-concept homodyne *en face* OCT system features measured axial and lateral resolutions of 14 μm (theoretical 8.7 μm) and 9.4 μm (theoretical 3.2 μm), respectively. The discrepancy between the measured and theoretical axial resolution can be attributed in part to the spectral variations in the power transfer coefficients of the 3×3 coupler, which we have assumed to be spectrally flat. The confocal parameter was measured as 97 μm. The signal-to-noise ratio (SNR) of the homodyne *en face* OCT is measured as 90 dB for a 10 μs integration time (the corresponding theoretical shot-noise-limited SNR is $\sim$102 dB). Figure 2 shows the theoretical (shot-noise-
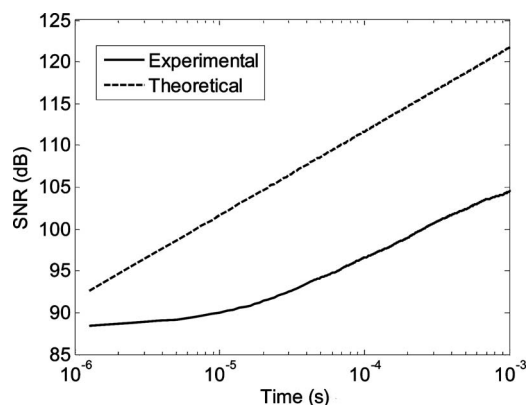
Fig. 2. Plots of theoretical (shot-noise-limited) as well as measured SNR versus integration time of the homodyne *en face* OCT system.
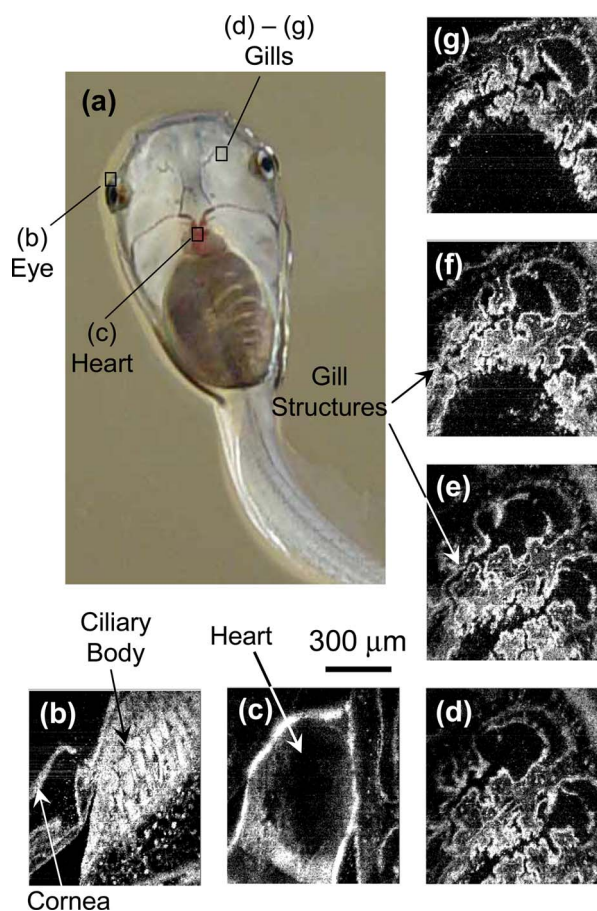

Fig. 3. (Color online) (a) Photograph of a stage 52 *Xenopus leavis* showing locations where *en face* images were acquired by using the homodyne OCT setup. Shown are the *en face* OCT images of (b) cornea and ciliary body in the eye, (c) heart, and (d) gill structures at a depth of 600 μm into the sample. (e)–(g) *En face* images of the gill region of (d) at 40 μm depth intervals into the sample. Each *en face* OCT image is ~790 μm×900 μm.

limited) as well as the measured SNR plots versus the integration time for our homodyne OCT system. The integration time is varied by simply accumulating the signal for the requisite time period. The dif-

ference in the SNR plots may be attributed to 3×3 coupler losses, signal loss due to the polarization mismatch between the sample and reference arms, and the remaining DC signal caused by variations in the interferometer coupling and the 3×3 coupler parameters over time because of temperature fluctuations. The effect of $1/f$ noise on the SNR is unclear at present and deserves further study.

We also demonstrate successful homodyne *en face* OCT imaging in a euthanized *Xenopus laevis* (stage 52) at a 600 μm depth inside the sample. Figure 3(a) is a photograph of the tadpole, indicating locations where *en face* OCT images were acquired. Figures 3(b)–3(d) show *en face* OCT images of tadpole heart as well as structures in the eye and the gill region. Figures 3(e)–3(g) show *en face* OCT images of the gill region [shown in Fig. 3(d)] at 40 μm depth intervals into the sample. The size of each *en face* OCT image is ~790 μm×900 μm. The data were acquired at 80 kHz, with a line scan rate of ~23 Hz. The data acquisition time per *en face* image was ~9 s. The measured SNR of the system at the image acquisition rate (80 kHz) is ~90 dB.

In conclusion, we have proposed and experimentally demonstrated, for the first time to our knowledge, a homodyne *en face* OCT system based on a 3 ×3 fiber-optic coupler. The system design is simple, easy to implement, highly sensitive, and allows for high-speed *en face* OCT imaging of highly scattering tissues and turbid media. Applications that can benefit from this simple imaging system include *en face* imaging of epithelial tissue layers of free surfaces of body for early detection and staging of near-surface microscopic precancerous lesions. We note that the proposed *en face* homodyne OCT system can be very easily integrated into a standard confocal microscope, hence leading to homodyne optical coherence microscopy that will benefit from all the advantages of homodyne detection (ease of implementation) and confocal microscopy (superior axial gating) as well as low coherence interferometry[7] (high SNR as well as better depth penetration by virtue of sharper coherence gate rejection).

Z. Yaqoob's e-mail address is zyaqoob@caltech.edu.

References

1. D. Huang, E. A. Swanson, C. P. Lin, J. S. Schuman, W. G. Stinson, W. Chang, M. R. Hee, T. Flotte, K. Gregory, C. A. Puliafito, and J. G. Fujimoto, Science **254**, 1178 (1991).
2. J. A. Izatt, M. R. Hee, G. M. Owen, E. A. Swanson, and J. G. Fujimoto, Opt. Lett. **19**, 590 (1994).
3. A. Dubois, L. Vabre, A. C. Boccara, and E. Beaurepaire, Appl. Opt. **41**, 805 (2002).
4. C. K. Hitzenberger, P. Trost, P. W. Lo, and Q. Y. Zhou, Opt. Express **11**, 2753 (2003).
5. E. Beaurepaire, L. Moreaux, F. Amblard, and J. Mertz, Opt. Lett. **24**, 969 (1999).
6. M. A. Choma, C. H. Yang, and J. A. Izatt, Opt. Lett. **28**, 2162 (2003).
7. R. C. Youngquist, S. Carr, and D. E. N. Davies, Opt. Lett. **12**, 944 (1987).